

Obscured Asymptotic Giant Branch stars in the Magellanic Clouds IV. Carbon stars and OH/IR stars*

Jacco Th. van Loon^{1,2}, Albert A. Zijlstra¹, Patricia A. Whitelock³, Peter te Lintel Hekkert⁴, Jessica M. Chapman^{5,6}, Cecile Loup^{7,8}, M.A.T. Groenewegen⁹, L.B.F.M. Waters^{2,10} and Norman R. Trams¹¹

¹ European Southern Observatory, Karl-Schwarzschild Straße 2, D-85748 Garching bei München, Germany

² Astronomical Institute, University of Amsterdam, Kruislaan 403, NL-1098 SJ Amsterdam, The Netherlands

³ South African Astronomical Observatory, P.O.Box 9, 7935 Observatory, Republic of South Africa

⁴ Australia Telescope National Facility, Parkes Observatory, P.O.Box 276, Parkes, NSW 2870, Australia

⁵ Anglo-Australian Observatory, P.O.Box 296, Epping, NSW 2121, Australia

⁶ Australia Telescope National Facility, P.O.Box 76, Epping, NSW 2121, Australia

⁷ European Southern Observatory, Casilla 19001, Santiago 19, Chile

⁸ Institut d'Astrophysique de Paris, 98bis Boulevard Arago, F-75014 Paris, France

⁹ Max-Planck Institut für Astrophysik, Karl-Schwarzschild Straße 1, D-85740 Garching bei München, Germany

¹⁰ Space Research Organization Netherlands, Landleven 12, NL-9700 AV Groningen, The Netherlands

¹¹ ISO Science Operations Centre, Astrophysics Division of ESA, Villafranca del Castillo, P.O.Box 50727, E-28080 Madrid, Spain

Received date; accepted date

Abstract. We present N -band photometry for a sample of 21 dust-enshrouded AGB stars in the Large Magellanic Cloud, and three additional sources in the Small Magellanic Cloud. Together with near-infrared photometry, this is used to give a tentative classification into carbon and oxygen-rich atmospheres. Bolometric luminosities are also estimated for these stars. In addition, we present the results of a survey for OH masers in the LMC, which resulted in the discovery of OH maser emission from IRAS04407–7000. Spectra between 600 and 1000 nm have been obtained for two heavily obscured AGB stars in the LMC, confirming them to be highly reddened very late M-type giants. Because the dust-enshrouded stars are clearly undergoing heavy mass loss they are assumed to be very near the termination of their respective Asymptotic Giant Branch phases. The fraction of mass-losing carbon stars decreases with increasing luminosity, as expected from Hot Bottom Burning. The best candidate carbon star, with $M_{\text{bol}} \sim -6.8$ mag, is the most luminous mass-losing carbon star in the Magellanic Clouds, and amongst the most luminous AGB stars. At lower luminosities ($M_{\text{bol}} \sim -5$ mag) both oxygen and carbon stars are found. This may be explained by a range in metallicity of the individual mass-losing AGB stars.

Key words: Stars: carbon – circumstellar matter – Stars: mass loss – Stars: AGB and post-AGB – Magellanic Clouds – Infrared: stars

1. Introduction

Luminous Asymptotic Giant Branch (AGB) stars in the Large Magellanic Cloud (LMC) were expected to become carbon stars as a result of third dredge-up of carbon to the stellar photosphere. The absence of carbon stars brighter than $M_{\text{bol}} \sim -6$ mag came therefore as a big surprise (Iben 1981). Hot Bottom Burning (HBB; cf. Iben & Renzini 1983) has been proposed as a mechanism to avoid producing luminous carbon stars by burning the carbon into nitrogen and oxygen before it reaches the stellar photosphere. Both third dredge-up and HBB are poorly understood phenomena, and better observational constraints on the theoretical models are required. It has been stated that in the LMC there is not only a deficiency of luminous carbon-stars, but a general deficit of AGB stars more luminous than $M_{\text{bol}} \sim -6$ mag: where a few hundred are expected, the observed number is a factor ten smaller (Frogel et al. 1990; Reid et al. 1990).

Until recently, searches for AGB stars in the MCs had been limited to optically bright stars (e.g. Blanco et al. 1980; Westerlund et al. 1981; Costa & Frogel 1996 and references therein). Such stars may evolve further

* based on observations obtained at the European Southern Observatory (La Silla, Chile: proposal ESO 54.E-0135), the South African Astronomical Observatory, and the Australia Telescope National Facility

along the AGB, changing luminosity, chemical composition and other (circum-)stellar parameters. On the upper AGB they experience heavy mass loss and become enshrouded in dust, making them practically invisible at optical wavelengths and accessible only in the infrared (IR) (see Habing 1996 for a review). These obscured AGB stars presumably represent the end product of AGB evolution, and can be used directly to test the predictions of stellar evolution theories. They may account for some fraction of the missing luminous AGB stars. The luminous carbon stars, that are absent in samples of optically visible AGB stars, might also be found amongst the obscured AGB stars.

After the IRAS satellite opened the thermal-IR window towards the MCs, the first samples of obscured AGB stars and red supergiants (RSGs) in the MCs were compiled (Whitelock et al. 1989; Reid 1991; Wood et al. 1992). We have significantly extended the sample of known obscured AGB stars in the MCs. In paper I (Loup et al. 1997) we selected IRAS point sources as candidate obscured AGB stars in the LMC. In paper II (Zijlstra et al. 1996) and paper III (van Loon et al. 1997) new near-IR (NIR) counterparts for a large subsample of these candidates were discussed. A total of 46 obscured AGB stars in the LMC and 5 in the SMC have now been identified, allowing a detailed study of the population of obscured AGB stars in the MCs to be made. In this paper we present the results of an attempt to classify these stars into oxygen and carbon stars, and to study their luminosity distributions.

Optically bright AGB stars are relatively easy to classify as carbon- or oxygen-rich from low-resolution spectra in the 500 to 800 nm region. In the NIR, carbon stars are often distinguished from oxygen stars by their ($J - K$) colours (e.g. Feast et al. 1982). These methods do not work for obscured AGB stars which are optically too faint, and whose NIR colours are more dependent on the optical depth of the circum-stellar envelope (CSE) than on the effective temperature (Feast 1996). For obscured stars, OH maser emission indicates an oxygen-rich CSE, but few evolved stars in the MCs have detectable OH masers (Wood et al. 1992) and this technique is of limited use in the LMC. The IRAS ($[25] - [60]$) versus ($[12] - [25]$) two-colour diagram may be used to separate carbon-rich CSEs from oxygen-rich CSEs (van der Veen 1989), but the MCs are too distant for the IRAS instruments to yield reliable $60 \mu\text{m}$ fluxes. Guglielmo et al. (1993) demonstrated the use of combined near- and mid-IR colour-colour diagrams in isolating carbon stars in the Milky Way. In papers II and III we confirmed that the ($K - [12]$) versus ($H - K$) or ($J - K$) diagram can be used successfully for the MCs. This is the principal method we use here to chemically classify our MC sample of obscured AGB stars, with in a few cases an optical spectrum or an OH maser detection too.

In Sect. 2 we present N -band photometry for 21 obscured AGB stars in the LMC, 2 in the SMC and the SMC red supergiant (RSG) or foreground star, VV Tuc. These stars form a subsample of the obscured AGB candidates in paper II. In Sect. 3 we discuss additional NIR photometry from SAAO for these sources. Sect. 4 describes the results of a search for OH maser emission from fields in the LMC, centred at known obscured AGB stars, trying to extend the known sample of OH/IR stars in the LMC (Wood et al. 1992). Sect. 5 presents optical/NIR spectra of obscured AGB stars in the LMC. In Sect. 6 we discuss the ($K - [12]$) versus ($H - K$) diagram used to classify the AGB stars according to the chemical type of their CSEs. We also study the position of the RSGs in this diagram. In Sect. 7 we derive bolometric luminosities, and investigate the time variability in the N -band. The luminosity distributions of the obscured AGB stars and the relative distributions of the carbon- and oxygen-rich stars are derived. We discuss the results and summarise the conclusions.

2. Mid-infrared imaging photometry

We used the ESO $10 \mu\text{m}$ camera TIMMI (Käufl et al. 1992) at the 3.6m telescope at La Silla on the nights of 1994 November 19/20 and 20/21 to obtain N -band photometry ($\lambda_0 = 10.10 \mu\text{m}$, $\Delta\lambda = 5.10 \mu\text{m}$). This filter is centred on the silicate dust feature, which is prominent in oxygen-rich CSEs. We chose a scale of $0.5''$ per pixel, giving a field of view of $32'' \times 32''$. Because of the very high background radiation the standard procedure for observing in the thermal IR is chopping and nodding. We used a chopper throw of $8''$, which insured that the source was in all of the frames, thereby increasing the signal-to-noise significantly.

Flat-fields were obtained by measuring the flux of a standard star at 13 positions uniformly distributed over the array, and fitting a two-dimensional parabola to the measured values. This gives reliable corrections over all but the very edges of the array. We followed the reduction procedure as it is described in paper II to derive magnitudes. This method is based on the sampling of the point-spread function for each star individually by means of (software-)aperture photometry with an increasing aperture size. The deduced magnitude profile is then compared to that of a standard star. In this way we obtained accurate and reliable magnitude measurements, as well as reliable error estimates.

The N -band magnitudes are listed in Table 1, along with their $1-\sigma$ error estimates, and the times of mid-exposure. The exposure times were typically between 10 and 30 min. In the case of a non-detection in the N -band, the $1-\sigma$ error indicates the probability that the source is actually brighter than the lower limit given in Table 1. We refer to Appendix A for a discussion about the photometric standard stars that are available for the N -band.

Table 1. Names, Heliocentric Julian Dates, K and N -band magnitudes, $(H - K)$ and $(K - [12])$ colours for the stars in our N -band photometry sample. We adopt $[12] = N - 0.33$ (see text). $1-\sigma$ error estimates are given.

IRAS	other	HJD-2 440 000	K	σ_K	N	σ_N	$(H - K)$	$\sigma_{(H-K)}$	$(K - [12])$	$\sigma_{(K-[12])}$
<i>SMC</i>										
00165-7418	VV Tuc	9677.62	7.1	0.3	4.67	0.06	0.24	0.10	2.76	0.3
00350-7436		9676.57	9.13	0.03	5.20	0.04	1.08	0.01	4.26	0.05
01074-7140	HV12956	9676.60	9.6	0.1	4.99	0.03	0.38	0.02	4.94	0.10
<i>LMC</i>										
04286-6937		9676.63	11.07	0.10	5.99	0.07	1.76	0.02	5.41	0.12
04374-6831		9676.67	12.42	0.05	6.09	0.07	2.46	0.02	6.66	0.09
04407-7000		9676.70	9.17	0.05	5.30	0.05	1.11	0.02	4.20	0.07
04496-6958		9676.72	8.84	0.02	5.03	0.04	1.40	0.01	4.14	0.04
04498-6842		9676.73	7.51	0.01	3.70	0.03	0.53	0.01	4.14	0.03
04539-6821		9676.76	12.7	0.1	5.81	0.06	2.7	0.2	7.22	0.12
04557-6753		9676.78	11.56	0.02	4.94	0.03	2.12	0.07	6.95	0.04
05003-6712		9677.71	10.8	0.2	5.89	0.10	1.56	0.10	5.24	0.22
05009-6616		9677.68	11.00	0.05	5.23	0.02	1.75	0.02	6.10	0.05
05099-6740	TRM023	9677.73	11.41	0.07	>6.86	0.23	1.19	0.01	<4.88	0.24
05112-6755	TRM004	9677.75	12.3	0.1	4.94	0.03	2.17	0.15	7.69	0.10
05112-6739	TRM024	9677.77	12.9	0.2	5.24	0.05	2.7	0.2	7.99	0.21
05117-6654	TRM072	9677.79	11.39	0.03	5.45	0.13	1.70	0.10	6.27	0.13
05128-6455		9677.80	10.36	0.02	4.93	0.04	1.53	0.02	5.76	0.04
05190-6748	TRM020	9677.82	12.4	0.1	4.86	0.03	2.9	1.0	7.87	0.1
05203-6638	TRM088	9677.84	10.50	0.03	6.00	0.09	1.65	0.02	4.83	0.09
05291-6700		9677.86	10.1	0.3	>6.99	0.28	0.97	0.10	<3.44	0.4
05329-6709	TRM060	9676.80	9.4	0.1	3.70	0.02	2.20	0.05	6.03	0.1
05348-7024		9676.81	14.4	1	5.17	0.02	4.9	1.0	9.56	1.0
05360-6648	TRM077	9676.84	13.9	1	6.30	0.08	2.8	0.6	7.93	1.0
05506-7053		9676.86	12.2	0.2	>6.14	0.11	2.4	0.2	<6.39	0.23

3. Near-infrared photometry

The N -band photometry is complemented by near-infrared (NIR) photometry from a project at SAAO to monitor dust-enshrouded Long Period Variables (LPVs) in the LMC. At this stage, we only derived NIR magnitudes and colours for the epoch of N -band measurement, from the monitoring data as it was available in 1996 March.

The NIR magnitudes measured at different epochs were interpolated to obtain estimates for the 1994 November epoch of the N -band measurement. The errors on the K magnitudes were estimated “by eye”. They depend on the degree to which the light curve is sampled, as well as on the accuracies of the individual measurements. The $(H - K)$ colour at the time of the N -band measurement was estimated by interpolating the $(H - K)$ colours as they had been measured at the different epochs, rather than interpolating H and K magnitudes separately and deriving $(H - K)$ from the interpolated magnitudes. The two values for the $(H - K)$ colour were always consistent with each other, indicating a reliable estimation of the accuracies of the estimated individual H and K magnitudes for the 1994 November epoch of the N -band measurement. The results are presented in Table 1. For the single epoch NIR photometry of IRAS00165-7418 we adopted formal

errors of 0.3 and 0.1 mag on K and $(H - K)$ respectively, in accordance with the expected variability (see below).

For IRAS05291-6700, IRAS05348-7024, and IRAS05360-6648 the IRAC2 data from paper II were used. We transformed the magnitudes from the IRAC2 system to the SAAO system (Carter 1990), using (Lidman 1995):

$$\begin{pmatrix} J_{\text{SAAO}} \\ H_{\text{SAAO}} \\ K_{\text{SAAO}} \end{pmatrix} = \begin{pmatrix} 1.125 & 0 & -0.125 \\ -0.032 & 1 & 0.032 \\ 0.059 & 0 & 0.941 \end{pmatrix} \times \begin{pmatrix} J_{\text{IRAC2}} \\ H_{\text{IRAC2}} \\ K_{\text{IRAC2}} \end{pmatrix} \quad (1)$$

For the reddest sources, the difference is of the order of a few tenths of a magnitude. The formal errors include the effects of the faintness of the source, the difference in epochs between the IRAC2 and TIMMI observations, the expected amplitude of variability, and the error introduced by the conversion from the IRAC2 to the SAAO photometric system. For IRAS05348-7024 we assumed an IRAC2 J -band magnitude of $J_{\text{IRAC2}} = 24$, to be able to calculate the transformation to the SAAO system. This value has been chosen to be consistent with the expected SAAO J -band magnitude (see Appendix B). The error introduced by this assumption will not dominate the error in the derived NIR magnitudes. The $(H - K)$ colour for IRAS05190-6748 has been estimated from the $(K - L)$

colour as described in the Appendix, adopting a formal error of 1.0 magnitude.

4. A search for OH maser emission from two LMC fields

The presence of a strong OH maser in a mass-losing star is direct evidence that the star is oxygen-rich. OH maser emission has previously been detected from six luminous AGB stars and RSGs in the LMC by Wood et al. (1992). Their detections, with the Parkes 64-m radio telescope with an OH detection level of ~ 60 mJy, suggested that the expansion velocities of OH/IR stars in the LMC are substantially lower than for OH/IR stars in the Milky Way. Zijlstra et al. (1996) and van Loon et al. (1996), however, found a difference of only ~ 20 to 30% at most. The OH (non-)detections demonstrated that the LMC OH/IR stars are likely to have optically thinner CSEs than their galactic counterparts. Less IR pumping, together with a lower oxygen abundance, may then lead to the low OH maser flux densities of the LMC sources.

In order to test whether OH maser emission could be detected from sources with lower infrared luminosities, we decided to search for OH maser emission at 1612 MHz, in two LMC fields of size 0.5×0.5 square degrees. The selected fields were centred at the two IRAS sources IRAS04407–7000 and IRAS05112–6755. IRAS04407–7000 is one of the brightest AGB stars in the LMC with an IRAS $12 \mu\text{m}$ flux density of 0.81 Jy, while IRAS05112–6755 is also an AGB star (paper II), with an IRAS $12 \mu\text{m}$ flux density of 0.41 Jy.

4.1. OH Observations

The OH maser observations were made with the Australia Telescope Compact Array (ATCA) on 1994 September 5 to 7. The ATCA is an east-west array of six 22-m antennas which has a maximum baseline of 6 km. For a wavelength of 18 cm, the angular resolution is approximately 6 arcsec.

The two fields, centred on the positions of IRAS05112–6755 and IRAS04407–7000, were observed for total on-source integration times of 10 and 3 hrs, respectively. The total spectral bandpass of 4 MHz was centred at 1611 MHz. It was split into 1024 spectral channels, giving a channel separation of 0.71 km s^{-1} , and a velocity resolution of 0.85 km s^{-1} . The data were corrected for atmospheric amplitude and phase variations using observations of strong nearby continuum sources. To calibrate the flux density scale, the primary calibrator source, 1934–638 was also observed. This was taken to have a flux density of 14.8 Jy at 18 cm.

The data were reduced using routines in the AIPS and MIRIAD radio-astronomy packages. As considerable interference from the Russian Glonass satellites was present during the observations, the visibility data for the shorter baselines were first edited to remove sections containing

Table 2. Names, radio positions, and heliocentric peak velocities (in km s^{-1}) of the (possible) OH detections.

Name	RA (2000.0)	Dec (2000.0)	v_{hel}
IRAS04407–7000	$04^{\text{h}}40^{\text{m}}28.5^{\text{s}}$	$-69^{\circ}55'14''$	239
#144	$04^{\text{h}}40^{\text{m}}19.3^{\text{s}}$	$-69^{\circ}57'44''$	266
#291	$04^{\text{h}}40^{\text{m}}34.3^{\text{s}}$	$-69^{\circ}51'19''$	244
#321	$04^{\text{h}}40^{\text{m}}14.0^{\text{s}}$	$-69^{\circ}50'31''$	226

strong interference. Glonass interference signals near 1612 MHz are generally detected on baselines below one km. After removing the interference the data were then Fourier transformed to the image plane.

4.2. Search strategy

To search for detections we constructed data cubes on the inner $16.3' \times 16.3'$ of the fields centred on each of the two IRAS sources, covering a velocity range of 170 to 340 km s^{-1} . Each cube consisted of $512 \times 512 \times 230$ pixels of size $2.5'' \times 2.5'' \times 0.73 \text{ km s}^{-1}$. Natural weighting was applied in deriving resolution matched spectra from this cube. In this way we achieved final RMS noise levels ($1-\sigma$) of 12 mJy and 6 mJy for the fields on IRAS04407–7000 and IRAS05112–6755 respectively.

The cubes were searched for all spikes above 4.7σ . This resulted in about 250 candidates which were inspected by eye. The number is consistent with Gaussian distributed noise. All of the spikes were single velocity-channel spikes and disregarded as noise. A filter was applied to the data allowing us to lower the threshold to 3.5σ . This filter demanded that three neighbouring velocity channels had a combination of fluxes equal or exceeding 1, 0.3 and 0.2 times the 3.5σ threshold. Around 450 candidates per field were recovered. This number is again consistent with random noise. Inspection of all individual spectra resulted in a list of a few dozen candidates, the best of which is #321 (our nomenclature).

4.3. OH detections

The candidates were checked for IRAS counterparts. None were found, except for the known obscured AGB star IRAS04407–7000 (see paper II). The positions of two other candidates are coincident with stars visible on ESO-POSS plates: #144 and #291. The spectra of four candidate OH-maser sources are shown in Fig. 1, and their parameters are given in Table 2. All detections peak with a flux density of about 0.05 Jy (a bit over 4σ). We conclude that one new OH/IR star (IRAS04407–7000) was detected, and that there may be up to a few dozen more OH/IR stars at a flux level of ~ 40 to 50 mJy. Current technology is able to detect only the brightest stellar masers at the distance of the MCs (Wood et al. 1992; van Loon et al. 1996). Any significant improvement in sensitivity would

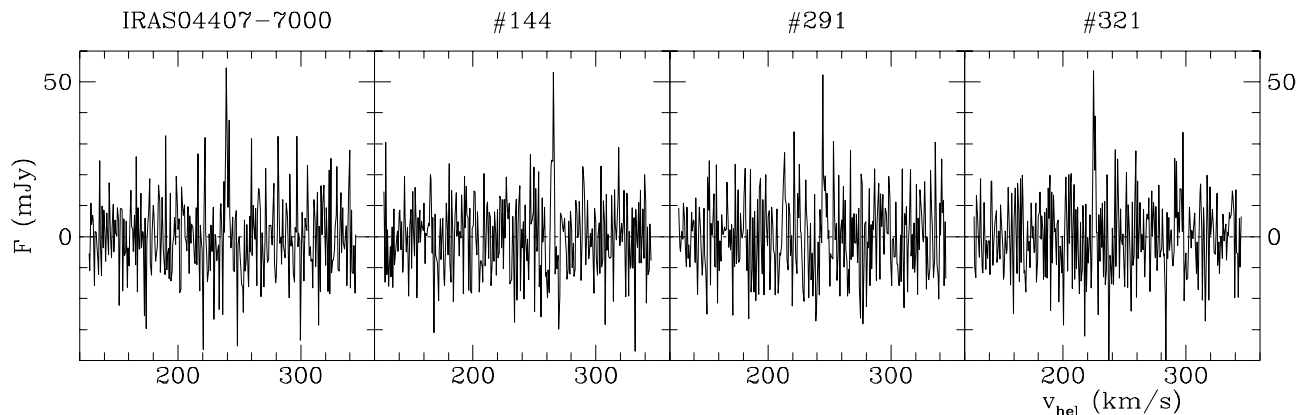


Fig. 1. Spectra of the 1612 MHz OH maser detection of IRAS04407-7000 (leftmost), and the candidate detections #144 (center left), #291 (center right), and #321 (rightmost)

therefore be expected to drastically increase the number of stellar masers known in the MCs.

5. Optical/NIR spectroscopy of IR stars in the LMC

We used the ESO 3.5m New Technology Telescope at La Silla on the night of 1996 February 4 to obtain low resolution ($R=500$) spectra, between 0.6 and 1 μm , of the stars IRAS04509-6922 and IRAS04516-6902, to chemically classify their photospheres. The stars were identified from their very red colours on V - and I -band acquisition images. The CCD frames were corrected for the electronic offset (bias) and for the relative pixel response (flatfield). The sky-subtracted spectra were then corrected for the wavelength dependence of the instrumental response, and for atmospheric extinction.

5.1. IRAS04509-6922 and IRAS04516-6902

The spectra of IRAS04509-6922 and IRAS04516-6902 are presented in Fig. 2. The strong TiO bands leave no doubt about their photospheres being oxygen rich. We show below that they are severely obscured by dusty CSEs. They are both luminous, large amplitude variables, with periods of 1290 and 1090 days respectively (Wood et al. 1992), making them good OH maser candidates. IRAS04516-6902 has not been searched for OH maser emission, while for IRAS04509-6922 Wood et al. (1992) derive an upper limit of 0.04 Jy, which is comparable to the fluxes from the new detection(s) discussed above. The only extra-galactic OH/IR star of which an optical spectrum had been taken so far is the extremely bright red supergiant IRAS04553-6825 (Elias et al. 1986).

We classify the two IR stars to half a subclass accuracy on the basis of the relative strengths of the various molecular bands at about 0.71, 0.77, 0.83, 0.84, and 0.89 μm

(TiO) and at about 0.74, 0.79, and 0.86 μm (VO), comparing with the representative spectra in Turnshek et al. (1985) and especially Fluks et al. (1994). We find very late types of M10 (IRAS04509-6922) and M9 (IRAS04516-6902). The relative strengths of the TiO bands in the 0.97 to 1.02 μm region, and the absence of FeH absorption at 0.99 μm indicate that these stars are giants not galactic dwarfs (Couture & Hardy 1993). Fluks et al. (1994) assign effective temperatures of ~ 2700 K and 2500 K to spectral types of M9 and M10 respectively, but it is not known how this depends on metallicity. Feast (1996) suggests that Mira variables may be different from other M-type stars in their relation between spectral type and effective temperature.

To quantify the reddening by the CSE, we compare the intensity levels in the spectrum at 0.70 μm and 0.84 μm between the programme star and a comparison star of the same spectral type. The spectral slope at these pseudo-continuum wavelengths is relatively flat over some 0.01 μm , and the result is therefore not very sensitive to the spectral resolution. There may be a slight metallicity effect, introduced by the TiO absorption bands at 0.84 μm , but this is probably small compared to the effects of extinction. Differential slit losses are not important, as the slit was positioned at the I -band stellar image and the spectra were taken at air masses smaller than 1.5.

We adopt an extinction curve $A_\lambda/E_{(B-V)}$ (Fluks et al. 1994, and references therein), and correct the $A_V = R \times E_{(B-V)}$ for the dependence on spectral type (Fluks et al. 1997, who calibrate to $R = 3.1$ for an O7.5V star). We measured the ratio of the intensities, at 0.70 μm and 0.84 μm , for the comparison spectra from Fluks et al. (1994) and for the programme stars: IRAS04509-6922 and IRAS04516-6902. From these ratios the extinction, A_V , is derived in magnitudes as it would be measured in the Johnson V -band (Table 3). The A_V estimation is accurate to within a magnitude. Thus it is clear that both stars suf-

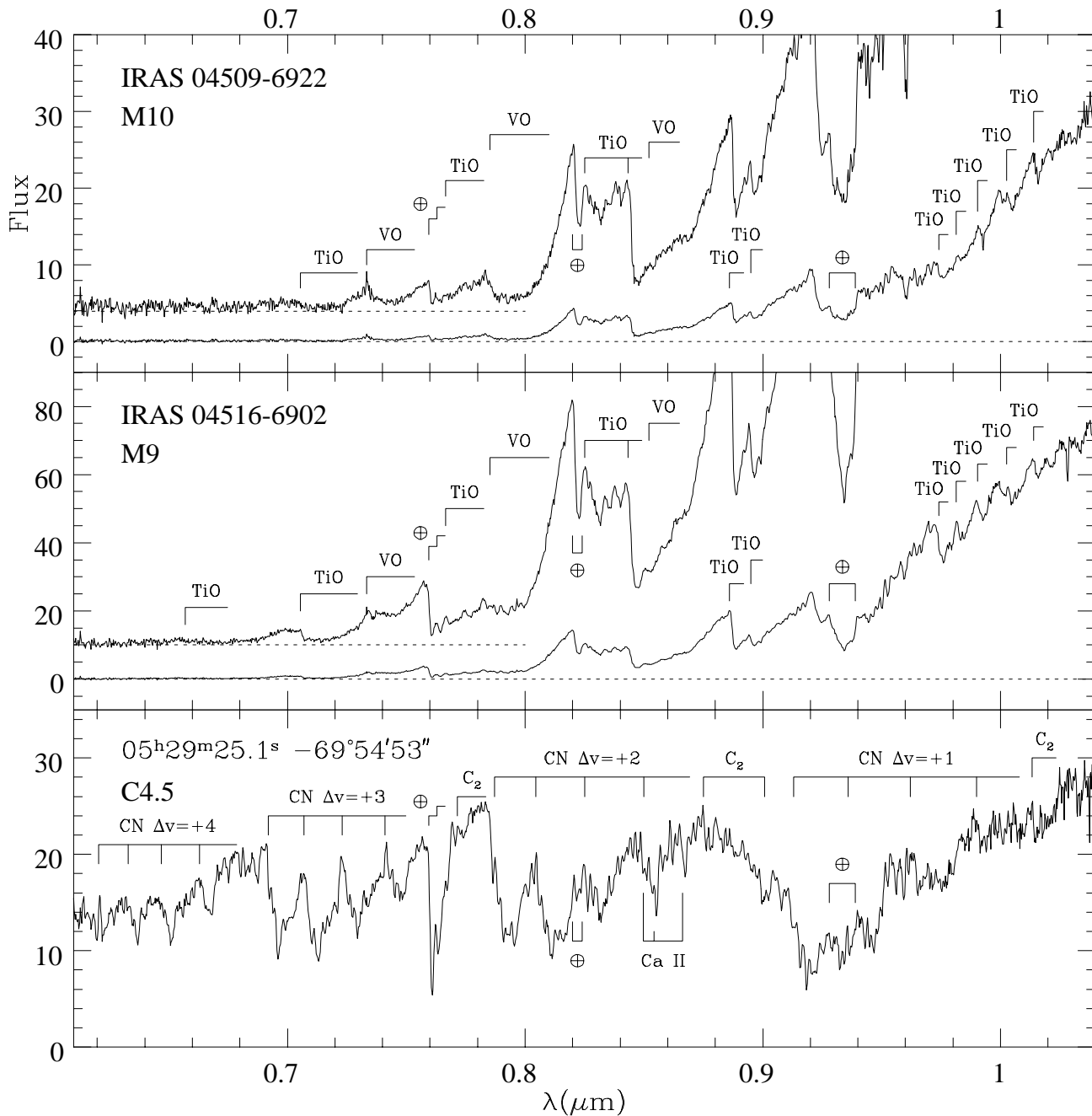


Fig. 2. Spectra of the IR stars IRAS04509–6922 and IRAS04516–6902, and of a serendipitously discovered carbon star of which the position is given in 2000 coordinates accurate to within $\sim 2''$. The spectra of the IR stars are displayed a second time, multiplied by 5 (and with a small offset in flux) to show better the heavily extinguished part around $0.7 \mu\text{m}$. The flux scales have not been calibrated. The main spectral features are indicated, including the strongest telluric absorption features

fer from significant circumstellar extinction, although less than do typical galactic OH/IR stars which have $A_V \gg 10$ mag (Habing 1996).

5.2. A cluster carbon star near IRAS05298–6957

The OH/IR star IRAS05298–6957 (Wood et al. 1992) could not be identified in the V - and I -band snapshots. It was probably considerably fainter than $I = 20$ mag (60 s acquisition exposure). Its location in the small star cluster

Table 3. Ratio of intensity levels in the spectrum at $0.70 \mu\text{m}$ and $0.84 \mu\text{m}$. They are estimated from the intrinsic spectra from Fluks et al. (1994), and from the spectra of the oxygen-rich IR stars shown here. For IRAS04509–6922 and IRAS04516–6902 the derived extinction in magnitudes for a Johnson V measurement is given.

Star	Spec.Type	$I_{0.70}/I_{0.84}$	A_V
Fluks et al.	M8	0.340	0
Fluks et al.	M9	0.250	0
Fluks et al.	M10	0.174	0
IRAS04509–6922	M10	0.09	3.4
IRAS04516–6902	M9	0.10	4.7

HS327 (Hodge & Sexton 1966) results in severe crowding and contributes to the difficulty in finding it.

However, a very red (in $V - I$) star was found at the Northern rim of the same cluster, about $22''$ from the position of the OH/IR. A spectrum of this star was obtained, in the same way as described in section 5.0, and is illustrated in Fig. 2. The numerous CN bands, e.g. at about 0.63 , 0.65 , 0.67 , 0.70 , 0.71 , 0.73 , 0.75 , 0.79 , and $0.92 \mu\text{m}$, and the weak C_2 absorption at about $1.02 \mu\text{m}$, leave no doubt that it is a carbon star. The very red colours which resulted in its discovery are probably a consequence of very strong C_2 bands shortward of $0.563 \mu\text{m}$. This absorption will considerably decrease the V -band flux.

Unfortunately, our spectral coverage does not include the 0.44 to $0.6 \mu\text{m}$ region, upon which most spectral classification is based (e.g. Keenan 1993). The star is not a galactic dwarf (cf. Green 1997): the CaH bands at about 0.638 and $0.639 \mu\text{m}$ are absent, the K I lines at 0.767 and $0.770 \mu\text{m}$ are weak, and the FeH line at $0.99 \mu\text{m}$ is weak or absent, all of which are enhanced in late-M dwarfs (Jaschek & Jaschek 1987; Turnshek et al. 1985; Couture & Hardy 1993). The equivalent width of the Ca II triplet component at $0.866 \mu\text{m}$ is $W_\lambda \sim 4.7 \pm 0.5 \text{ \AA}$, suggesting it is a giant not a dwarf (Danks & Dennefeld 1994 and references therein). This is confirmed by the absence of strong absorption by the Na I doublet around $0.819 \mu\text{m}$ (Alloin & Bica 1989). A ^{13}C isotope super-enhancement, characteristic of J-type carbon stars, is not observed: the CN and C_2 bands at 0.606 and $0.619 \mu\text{m}$ are much stronger than their ^{13}C isotopic equivalents at 0.626 and $0.617 \mu\text{m}$ (Richer et al. 1979). $H\alpha$ is only barely visible, unlike the strong $H\alpha$ absorption seen in CH stars (Barnbaum et al. 1996). The Ba II absorption at $0.65 \mu\text{m}$ is much weaker than in barium stars. The strong CN absorption between ~ 0.6 and $0.8 \mu\text{m}$ is suggestive of an N-type star (i.e. a star on the thermally pulsing AGB) rather than of an R-type. We conclude that the spectral type is C4.5, estimated to half a subtype accuracy by comparison with spectra from Turnshek et al. (1985) and from Barnbaum et al. (1996).

The observed wavelengths of the Ca II triplet lines suggest a large radial velocity for the star ($\sim 300 \pm 100 \text{ km s}^{-1}$) consistent with membership of the LMC. The

flux scales of the spectra are not calibrated absolutely, mainly because of unknown slit losses and variable seeing. With uncalibrated acquisition images and the lack of NIR photometry, the bolometric luminosity of the carbon star remains unknown. The apparent association of both an OH/IR star and a carbon-star with a cluster is sufficiently interesting that it is important to ascertain if both are actually members. If they are, then the implications of a single population producing an AGB carbon-star and an OH/IR star at the same time will need serious consideration.

6. Carbon stars in a ($K - [12]$) versus ($H - K$) diagram

6.1. The Milky Way

In Fig. 3 we present the ($K - [12]$) versus ($H - K$) diagnostic diagram. This is used to distinguish between carbon- and oxygen-rich stars within the galactic sample of carbon stars (Fig. 3a) and oxygen stars (Fig. 3b) that Guglielmo et al. (1993) selected to test the diagnostic value of IR colour-colour diagrams. We adopt $[12] = -2.5 \log(S_{12}/28.3)$, where S_{12} is the flux density in Jy in the IRAS $12 \mu\text{m}$ band (IRAS Explanatory Supplement 1988). The original NIR photometry of Guglielmo et al. is on the ESO system, but we transformed their data to the SAAO system (Carter 1990). The carbon-star sequence (dotted straight line) is described by the empirical relation

$$(H - K) = 0.3 \times (K - [12]) \quad (2)$$

It is remarkable how well this extremely simple relation holds. The oxygen star sequence (solid curved line) approximately satisfies

$$(H - K) = 0.2 + 0.03 \times (K - [12])^2 + 0.0002 \times (K - [12])^4 \quad (3)$$

Although less simple than for the carbon-star sequence, the relation for oxygen stars is also described by a smooth polynomial. The deviation of the oxygen stars from the carbon star sequence for $(K - [12]) < 7$ mag is caused by the additional emission of the $10 \mu\text{m}$ SiO feature from the dusty CSE, while the deviation for $(K - [12]) > 7$ mag is due to additional absorption by the $10 \mu\text{m}$ SiO feature.

The data of Guglielmo et al. (1993) show that in the region of the ($K - [12]$) versus ($H - K$) diagram at $5 < (K - [12]) < 9$ mag and $1.3 < (H - K) < 3$ mag there are many more carbon stars (86) than oxygen stars (30). In Fig. 3 carbon stars are found rather evenly spread along their sequence, whereas oxygen stars are rarely found with $(H - K) > 2$ mag. Moreover the scatter of the most obscured oxygen stars in the ($K - [12]$) versus ($H - K$) diagram is substantial.

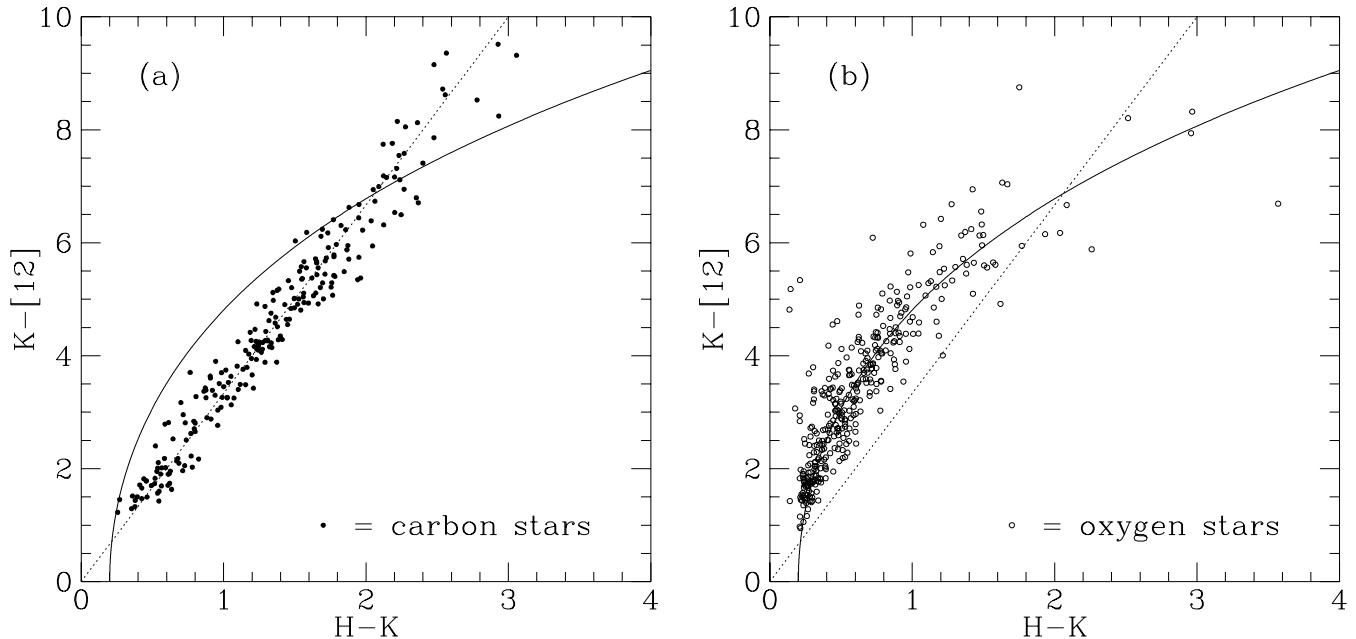


Fig. 3. $(K - [12])$ versus $(H - K)$ diagram for the carbon stars (a) and oxygen stars (b) of the galactic sample of Guglielmo et al. (1993). The dotted line and the solid curve are the empirical carbon- and oxygen-star sequences, respectively (see text)

6.2. Magellanic Clouds

In paper II we showed that the $(K - [12])$ versus $(H - K)$ diagnostic diagram may also be applicable to our sample of obscured AGB stars in the LMC. However, the uncertainties in the IRAS fluxes were too large to enable an individual separation into carbon and oxygen stars. Now that we have obtained accurate N -band magnitudes we are able to perform a diagnosis of the C/O abundance ratio for individual stars in our sample. Comparison of the N -band magnitudes with the IRAS $12\ \mu\text{m}$ flux densities (paper II) results in $(N - [12]) = 0.33 \pm 0.11$ mag, with no evidence for a colour term. The uncertainty given is the uncertainty in the estimation of the mean. Individual values can be off by a magnitude, but this we attribute to variability of the sources between the IRAS and N -band epochs (see section on variability) rather than uncertainties in the derived relation. The derived $(K - [12])$ colours are listed in Table 1 for the epochs of the N -band measurements.

All the stars in our sample are displayed in the $(K - [12])$ versus $(H - K)$ diagram (Fig. 4, large symbols), superimposed with the galactic carbon-star sequence (dotted straight line) and the galactic oxygen-star sequence (solid curved line). We also display the other AGB stars and the RSGs from the LMC and SMC as listed in paper II (Fig. 4, small symbols). Elias et al. (1985) presented $10\ \mu\text{m}$ photometry of a small subset of their sample of RSGs in the MCs, obtained at CTIO. We treated their $10\ \mu\text{m}$ magnitudes as if they were TIMMI N -band magnitudes,

and they are included in Fig. 4 for comparison (solid dots and crosses for LMC and SMC members, respectively). All data are on the SAAO photometric system, after applying transformation equations from Carter (1990) and McGregor (1994) where required. Some stars are confirmed to be oxygen rich, by our narrow-band photometry (paper II) or by our optical/NIR spectroscopy (shaded symbols), or by the detection of OH-maser radiation (bold symbols).

6.3. Classification by chemical type

We tentatively classify the stars of our N -band photometry sample as oxygen rich or carbon rich. The results are given in Table 4. Three stars are probably carbon rich (C). Nine other stars have been labeled “OC” because the type could not be determined. They are situated in a region of the $(K - [12])$ versus $(H - K)$ diagram where both carbon and oxygen stars are found — especially in the region around the carbon-star sequence between $(H - K) = 1.3$ and $(K - [12]) = 5$ mag, and $(H - K) = 3$ and $(K - [12]) = 9$ mag. All other stars of our sample are probably oxygen rich (O).

We sample well up to the intersection of the oxygen- and carbon-star sequences at $(K - [12]) \sim 7$ mag, where the $10\ \mu\text{m}$ SiO feature in oxygen stars is thought to go into absorption. Thus, at $(H - K) \sim 5$ mag IRAS05348-7024 must be an oxygen star with strong $10\ \mu\text{m}$ absorption. The apparent scarcity of stars with $(H - K) > 3$ mag is an effect of incompleteness, as the deepest NIR search so far

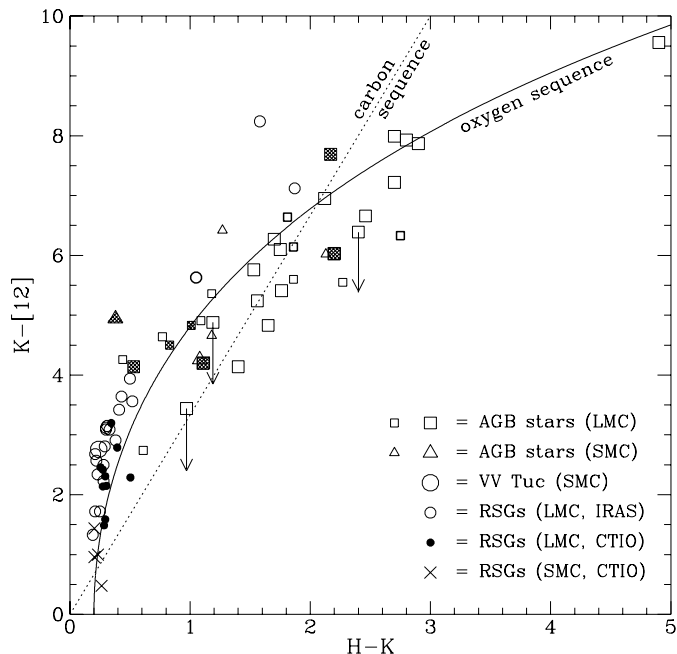


Fig. 4. $(K - [12])$ versus $(H - K)$ diagram for the stars of our sample (large symbols), and the other stars from paper II (small symbols). All NIR data is on the SAAO photometric system. We adopt $[12] = -2.5 \log(S_{12}/28.3)$, where S_{12} is the flux density in Jy in the IRAS 12 μm band (IRAS Explanatory Supplement 1988). Highlighted are OH masers (bold-faced symbols), and stars that are classified as oxygen stars either from the narrow-band photometry of paper II or from our optical/NIR spectroscopy (shaded symbols). Also plotted are RSGs in the LMC (solid dots) and SMC (crosses) with 10 μm photometry obtained at CTIO (Elias et al. 1985). The dotted line and the solid curve are the galactic carbon- and oxygen-star sequences respectively

(paper III) has revealed several of these highly obscured stars.

OH maser emission was detected from IRAS05329–6709 (Wood et al. 1992) and from IRAS04407–7000 (see above). This establishes their status as oxygen rich, since strong OH maser emission is not expected from carbon stars. The moderate expansion velocity, of about 12 km s^{-1} , of the OH-masing shell around IRAS05329–6709 suggests that it is an AGB star, not a red supergiant (RSG). The narrow-band mid-IR photometry (paper II) for these two stars, as well as for IRAS01074–7140, IRAS04498–6842 and IRAS05112–6755 also lead us to classify these stars as oxygen rich. A mid-IR spectrum of IRAS05329–6709 (Groenewegen et al. 1995) directly confirms it to be oxygen rich. Convolution of this spectrum with the response curves of the TIMMI narrow-band filters, and comparison with a flat spectrum representing an A0 V star yields colours $([9.8] - [11.3]) = 0.33 \text{ mag}$ and $([N] - [9.8]) = -0.22 \text{ mag}$ with a crudely estimated accuracy of 0.1 mag. This agrees within the estimated

Table 4. Classification of the stars in our N -band photometry sample as oxygen rich (O), carbon rich (C) or unknown (OC).

O	OC	C
<i>Small Magellanic Cloud</i>		
00165–7418	00350–7436	
01074–7140		
<i>Large Magellanic Cloud</i>		
04374–6831	04286–6937	
04407–7000		04496–6958
04498–6842		
04539–6821	04557–6753	
	05003–6712	
	05009–6616	
	05099–6740	
05112–6755		
	05112–6739	
	05117–6654	
	05128–6455	
05190–6748		05203–6638
		05291–6700
05329–6709		
05348–7024		
05360–6648		
05506–7053		

errors with the colours, $([9.8] - [11.3]) = 0.41 \text{ mag}$ and $([N] - [9.8]) = -0.02 \text{ mag}$, derived from the narrow-band photometry (paper II).

The two stars IRAS04509–6922 and IRAS04516–6902 were shown, from the spectra discussed above, to be oxygen rich. Their $(H - K)$ and $(K - [12])$ colours from Wood et al. (1992), after transformation to the SAAO system (McGregor 1994), place them very nicely on the oxygen-rich sequence, in a region where the 10 μm SiO feature is in emission. These stars are thus indeed experiencing mass loss, confirming that their extinction is circumstellar rather than interstellar.

The position of the SMC source IRAS00165–7418 (VV Tuc) at $(K - [12]) = 2.76$ and $(H - K) = 0.24$ is consistent with its classification as a mass-losing RSG in the SMC (see next section), rather than as a foreground star. The position of the SMC source IRAS01074–7140 in the $(K - [12])$ versus $(H - K)$ diagram suggests it may be a post-AGB star (cf. van Loon et al. 1997). The blue $(H - K)$ colour may reflect a higher effective temperature than an AGB star has, while there is still a considerable amount of 12 μm emission from the CSE. Alternatively, it may still be on the AGB, but have interrupted its mass loss recently following a thermal pulse. A similar scenario has been suggested for certain galactic stars by Whitelock et al. (1995).

The $(K - [12])$ versus $(H - K)$ diagram indicates that IRAS04496–6958 is a very good candidate carbon star. A preliminary analysis of a $3 \mu\text{m}$ spectrum that we obtained with the IR spectrometer at the CTIO 4m telescope in December 1996 indeed confirms the carbon-rich nature of the CSE of IRAS04496–6958.

We take the general agreement between the $(K - [12])$ versus $(H - K)$ diagram and more direct observational diagnostics as a justification for the use of the $(K - [12])$ versus $(H - K)$ diagram in chemically classifying obscured AGB stars in the MCs.

6.4. Red supergiants

The RSGs in the LMC, detected by IRAS, form a sequence that is slightly shifted to bluer $(H - K)$ or redder $(K - [12])$ with respect to the galactic sample of the stars from Guglielmo et al. (1993). The sample of Guglielmo et al. contains mainly AGB stars with few RSGs, because their stars were selected outside of the galactic plane. Thus mass-losing RSGs appear to have different IR colours than mass-losing AGB stars. At a given mass-loss rate, RSGs may have similar $12 \mu\text{m}$ flux densities to AGB stars, but the RSGs may be less obscured because of a greater inner radius of their CSEs. This would yield similar $(K - [12])$ colours, but smaller $(H - K)$ colours for the RSGs. This may also explain the large IR excess of the RSG IRAS05216–6753, compared to its NIR extinction: $(H - K) = 1.58$ and $(K - [12]) = 8.24$ mag. The effect is less visible in the IR colours of the RSGs from Elias et al. (1985), because these stars have lower mass-loss rates and therefore less $10 \mu\text{m}$ emission from a CSE.

Some stars we have classified as being on the AGB may actually be RSGs, and vice versa. The candidate AGB star IRAS04498–6842 may be an example of such a misclassification, as it was very luminous at the epoch of the N -band measurement (see below): it has $(K - [12])$ and $(H - K)$ colours which perfectly match the corresponding colours of the RSGs in the LMC. The same is true for IRAS05316–6604 (WOH SG374) at $(H - K) = 0.44$ and $(K - [12]) = 4.26$ mag.

The datum at $(H - K) = 0.61$ and $(K - [12]) = 2.74$ mag is WOH SG061 (SHV0453582–690242). Westerlund et al. (1981) selected this star on the basis of objective-prism spectra indicating an M-type. This spectral type was confirmed by Hughes & Wood (1990) using low-dispersion optical/NIR spectroscopy. In paper II we found it to be an AGB star, rather than a RSG. In the $(K - [12])$ versus $(H - K)$ diagram WOH SG061 follows the sequence for oxygen stars on the AGB as observed in the Milky Way. As the red $(H - K)$ colour of WOH SG061 with respect to the RSGs in the LMC is not due to a carbon-rich CSE or photosphere, we conclude that indeed mass-losing AGB stars in the LMC have redder $(H - K)$ colours than mass-losing RSGs in the LMC.

7. Luminosities

7.1. Variability

The stars can make excursions through colour-colour diagrams due to their intrinsic variability. For five stars we obtained N -band photometry in 1993 December (paper II): IRAS01074–7140, IRAS04407–7000, IRAS04498–6842, IRAS05112–6755, and IRAS05329–6709 (all probably oxygen stars). We can now compare these near- and mid-IR magnitudes and colours with those measured in 1994 November (Table 5). The K and $(H - K)$ for 1993 December have been estimated in the same way as for 1994 November (see above).

The mean difference (“1994 – 1993”) of the N -band magnitudes of the five stars is -0.2 ± 0.2 mag; there is no indication for a large systematic difference in the N -band measurements at the two epochs. Assuming a sinusoidal light-curve, the difference between the measurements at two random epochs is expected to be a fraction, $1/\pi$, of the peak to peak amplitude. We assume that the five difference measurements sample the light curve of a typical mass-losing oxygen-rich AGB star. This seems reasonable, considering the time span of nearly a year between the two epochs of measurement, and typical periods of variability of the order of one to four years. We thus find the mean peak to peak amplitude (Table 5).

The variability near $10 \mu\text{m}$ can also be estimated from a comparison between the N -band measurements (from 1994 November) and the IRAS fluxes. The latter do not represent the mean fluxes of the stars, neither are they entirely single-epoch. This is, however, not important when estimating the typical amplitude of variability, since the IRAS epoch is certainly very different from the N -band epoch. In Table 6 we list the magnitude differences between the $12 \mu\text{m}$ magnitudes derived from our N -band measurements and those derived from the IRAS data. The mean absolute value of these differences for the LMC stars is 0.43 mag. Hence the inferred typical amplitude of variability at $12 \mu\text{m}$ is 1.4 mag, which is in excellent agreement with the value we estimated from the N -band data in Table 5.

The K - and N -band magnitudes vary considerably, while the $(H - K)$ colours do not vary much. The $(K - [12])$ colours vary significantly, but not more than do the K - or N -band magnitudes. Thus the K - and N -band magnitudes vary neither in phase, nor in anti-phase. The phase difference can be estimated by simple vector calculus on the amplitudes of the K - and N -band magnitudes and $(K - [12])$ colours. In this way we estimate that either of the N - or K -band magnitudes follows the other with a phase-lag of about $\pi/4$, corresponding to a time-lag of $1/8$ period. Although based on five measurements only, the $(K - [12])$ differences between the two epochs correlate very well with the mean $(H - K)$ colours: the $(K - [12])$ colour becomes less variable as the CSE becomes optically thicker (larger $(H - K)$).

Table 5. Difference of the near and mid-IR magnitudes and colours between the 1994 November and 1993 December measurements for the stars in our sample for which we have N -band measurements at both epochs. Δ refers to (1994 value)–(1993 value). We also derived an estimation for the typical magnitude difference between minimum and maximum (amplitude, see text).

IRAS	K ('93)	ΔK	$(H - K)$ ('93)	$\Delta(H - K)$	N ('93)	ΔN	$(K - [12])$ ('93)	$\Delta(K - [12])$
01074–7140	9.90 ± 0.10	-0.30 ± 0.14	0.44 ± 0.05	-0.06 ± 0.05	5.78 ± 0.04	-0.79 ± 0.05	4.45 ± 0.11	0.49 ± 0.15
04407–7000	8.93 ± 0.01	0.24 ± 0.05	0.89 ± 0.01	0.22 ± 0.02	4.76 ± 0.02	0.54 ± 0.05	4.50 ± 0.03	-0.30 ± 0.07
04498–6842	7.84 ± 0.01	-0.33 ± 0.01	0.64 ± 0.01	-0.11 ± 0.01	3.67 ± 0.02	0.03 ± 0.04	4.50 ± 0.03	-0.36 ± 0.04
05112–6755	13.20 ± 0.10	-0.90 ± 0.14	1.93 ± 0.15	0.24 ± 0.22	5.56 ± 0.05	-0.62 ± 0.06	7.97 ± 0.11	-0.28 ± 0.15
05329–6709	9.80 ± 0.4	-0.04 ± 0.4	2.24 ± 0.20	-0.04 ± 0.20	3.91 ± 0.02	-0.21 ± 0.03	6.22 ± 0.4	-0.19 ± 0.4
amplitude		1.1		0.4		1.4		1.0

Table 6. J , H , K , and L -band magnitudes, and 12 and 25 μm flux densities for the epoch of the N -band measurements, the magnitude difference between the 12 μm flux densities at the N -band epoch and the 12 μm flux densities from IRAS, and the derived apparent and absolute bolometric magnitudes and luminosities for the stars for which we present N -band photometry. Brackets denote values derived from empirical colour relationships (see Appendix).

IRAS	J	H	K	L	S_{12} (Jy)	S_{25} (Jy)	$([12]_N - [12]_{\text{IRAS}})$	m_{bol}	M_{bol}	$\log(L/L_{\odot})$
00165–7418	8.30	7.40	7.10	6.80	0.52	0.33	0.00	9.66	−9.12	5.54
00350–7436	11.50	10.21	9.13	7.79	0.32	0.23	−0.07	11.96	−6.82	4.62
01074–7140	11.00	10.10	9.70	9.00	0.39	0.42	0.06	11.83	−6.95	4.67
04286–6937	15.30	12.82	11.07	9.00	0.15	0.12	0.39	13.18	−5.29	4.00
04374–6831	(18.04)	14.87	12.42	9.59	0.14	0.13	0.33	13.48	−4.99	3.88
04407–7000	11.93	10.26	9.17	7.93	0.29	0.24	1.11	12.07	−6.40	4.45
04496–6958	12.12	10.23	8.84	7.31	0.37	0.33	0.00	11.71	−6.76	4.59
04498–6842	9.18	8.03	7.51	6.62	1.27	1.19	−0.08	10.27	−8.20	5.17
04539–6821	(18.93)	15.50	12.70	9.70	0.18	0.21	−0.06	13.25	−5.22	3.98
04557–6753	(16.46)	13.66	11.56	9.10	0.41	0.34	−0.48	12.47	−6.00	4.29
05003–6712	14.20	12.40	10.80	9.20	0.17	0.17	1.04	13.09	−5.38	4.04
05009–6616	15.00	12.80	11.10	8.70	0.31	0.26	−0.19	12.59	−5.88	4.24
05099–6740	14.49	12.61	11.41	10.10	<0.07	<0.16	>1.1	13.81	−4.66	3.75
05112–6755	(17.15)	14.30	12.30	8.90	0.41	0.33	−0.01	12.46	−6.01	4.29
05112–6739	(19.13)	15.70	12.90	9.80	0.31	0.16	0.08	12.91	−5.56	4.11
05117–6654	(15.15)	12.80	11.39	9.00	0.25	(0.25)	−0.57	12.80	−5.67	4.16
05128–6455	13.50	11.80	10.36	8.40	0.41	0.60	−1.09	12.16	−6.31	4.41
05190–6748	(18.84)	(15.25)	12.40	9.00	0.44	0.30	−0.27	12.44	−6.03	4.30
05203–6638	14.50	12.10	10.50	8.70	0.15	(0.15)	0.05	12.98	−5.49	4.08
05291–6700	13.10	11.10	10.10	8.80	<0.06	<0.19	>0.14	13.11	−5.36	4.03
05329–6709	15.70	11.60	9.40	7.30	1.27	2.73	−0.44	10.90	−7.57	4.92
05348–7024	(25.10)	19.30	14.40	(8.65)	0.33	0.19	0.41	12.64	−5.83	4.22
05360–6648	19.70	16.60	13.90	(10.60)	0.12	0.12	0.70	13.84	−4.63	3.74
05506–7053	(17.60)	14.50	12.20	8.80	<0.13	<0.14	>1.7	13.24	−5.23	3.98

7.2. Bolometric luminosities

We have re-determined the bolometric luminosities for two reasons. First, the N -band measurements are generally of higher accuracy than the IRAS 12 μm flux densities. Secondly, we wish to determine the bolometric luminosities for the particular epoch of our N -band measurements. When IRAS flux densities and NIR magnitudes of large amplitude variables are obtained at different epochs their combination may result in an erroneous bolometric luminosity.

The NIR magnitudes have been estimated as described above. The 12 μm flux densities have been determined

from the N -band magnitudes, using $(N - [12]) = 0.33$ mag. The 25 μm flux densities have been derived from these new 12 μm flux densities, assuming the same ratios of 25 to 12 μm flux densities as observed by IRAS (paper II). Values in brackets have been estimated from the relations between the appropriate $(J - H)$, $(K - L)$, $([12] - [25])$, and $(H - K)$ colours (see Appendix), where $([12] - [25]) = -2.5 [\log(S_{12}/S_{25}) + \log(6.73/28.3)]$ (IRAS Explanatory Supplement 1988).

Bolometric luminosities were obtained by integrating under a spline-curve as described in paper II (with photometric zero-points from Glass & Feast 1973). We adopted

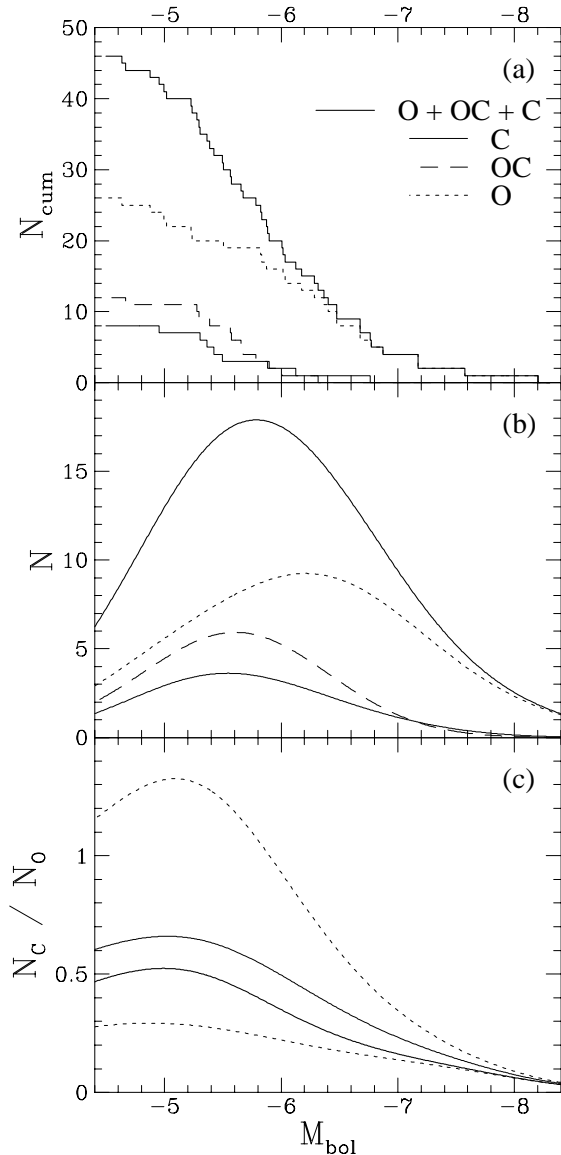


Fig. 5. (a) Cumulative distribution function of the full sample of IRAS detected AGB stars in the LMC over absolute bolometric magnitude: “oxygen” stars (dotted), “oxygen or carbon” stars (dashed), “carbon” stars (solid), and their sum (bold solid). (b) Applying Gaussian broadening (see text), we derive the distribution functions N . (c) From this we derive the distribution function of the ratio of carbon to oxygen stars for the two extreme cases of carbon star favoured (all OC stars are C stars) and oxygen star favoured (all OC stars are O stars), indicated by the dotted line. We also plot the ratio derived without assuming anything about the OC stars (bold solid), and assuming half of the OC stars are C stars (thin solid)

distance moduli of $(m - M)_0 = 18.47$ mag for the LMC and $(m - M)_0 = 18.78$ mag for the SMC (Feast and Walker 1987). Both lower and higher values for the distance moduli have appeared in the recent literature (e.g. Crotts et al. 1995; Gallagher et al. 1996; Sonneborn et al. 1997; Feast 1997; Caputo 1997; van Leeuwen et al. 1997; Feast

& Catchpole 1997), and from this we estimate the distance modulus to be known to about ± 0.15 mag. The accuracies of the individual bolometric luminosities are estimated to be typically 0.1 mag, plus the systematic error in the assumed distance moduli. The contribution to the uncertainty in the bolometric luminosity from the sometimes poorly known $25 \mu\text{m}$ flux density is less than 0.1 mag. The bolometric luminosity is also expressed in terms of solar luminosity, where we adopt for the solar absolute bolometric magnitude $M_{\text{bol},\odot} = 4.72$ mag (e.g. Sterken & Manfroid 1992). The results are enumerated in Table 6.

7.3. Luminosity functions

We combined the mass-losing AGB stars from the present sample with the remaining AGB stars from papers II & III. IRAS05283–6723 (TRM045) was omitted because of its uncertain identification. For IRAS05003–6712 we took the data quoted here, not that from paper III, because now we have simultaneous near- and mid-IR photometry. The chemical types of the remaining sources from paper II are estimated from the $(K - [12])$ and $(H - K)$ colours, or from additional data mentioned in paper II. All of the remaining paper II sources are found to be oxygen rich, except for IRAS00554–7351 which is a confirmed carbon star (Wood et al. 1992), and IRAS05295–7121 which could be either oxygen- or carbon-rich.

The cumulative distribution function of the different types of IRAS detected AGB stars in the LMC over absolute bolometric magnitude is presented in Fig. 5a. We apply Gaussian broadening by replacing each star with absolute bolometric magnitude $M_{\text{bol},\star}$ by

$$n = n_{\text{norm}} \times \exp\{-(M_{\text{bol}} - M_{\text{bol},\star})^2\} \quad (4)$$

where $n_{\text{norm}} = 0.564$ mag, to normalise to unity per star. The FWHM of the star has thereby become 0.83 mag. This is justified by both the variability of the sources and the small number of sources in our sample, and is necessary for deriving the distribution function over absolute bolometric magnitude (Fig. 5b).

From the distribution functions, we derived the dependence of the ratio of carbon to oxygen stars, on the absolute bolometric magnitude (Fig. 5c). Two extreme cases are plotted (dotted): the carbon-favoured case, in which all stars classified as “oxygen or carbon” stars turn out to be carbon rich, and the oxygen-favoured case, in which they are all oxygen rich. We may expect that the category of OC stars is composed of a mixture of both carbon and oxygen stars. We therefore also plot the trend that follows from assuming that half of the OC stars are oxygen stars and the other half carbon stars (solid), as well as the trend that follows from the probable oxygen and carbon stars only (bold solid).

8. Discussion

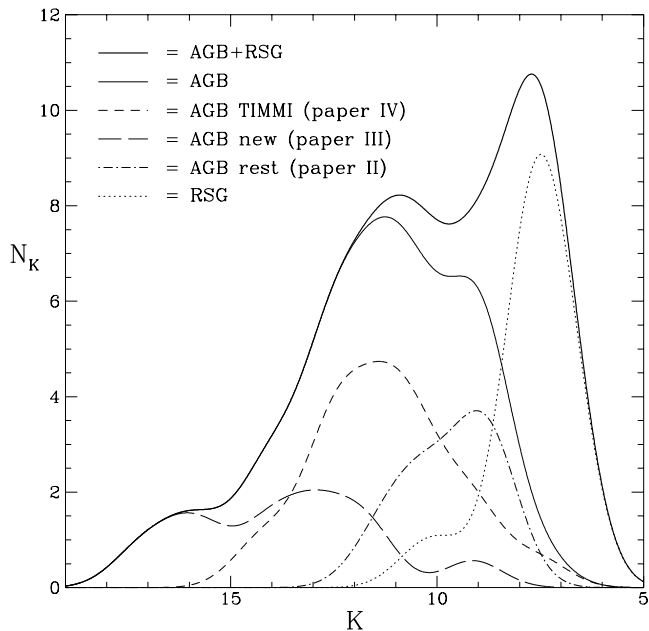


Fig. 6. Distribution functions N_K over apparent K magnitude, of IRAS detected LMC stars that have been identified with AGB stars and RSGs (see text): all known at present (bold solid), all AGB stars known at present (thin solid), TIMMI sample of AGB stars presented in this work (short dashed), new AGB stars presented in paper III (long dashed), remainder of presently known AGB stars (dot-dashed; see paper II), and all RSGs known at present (dotted)

8.1. Completeness and selection effects

Reid et al. (1990) used V - and I -band imaging to search for stellar counterparts of IRAS sources in the LMC. Many of these stars, however, are undetectable at wavelengths below $\sim 1\mu\text{m}$. We searched for IRAS sources at NIR wavelengths, and found ~ 20 mass-losing AGB stars more luminous than $M_{\text{bol}} \sim -6$ mag. Are there more?

In Fig. 6 we plot the distribution functions over apparent K -band magnitude, of stars that have been detected by IRAS and that subsequent searches have revealed to be AGB stars or RSGs in the LMC. We applied Gaussian broadening as before. Stars found in I -band searches are generally optically thin in the K -band, and the K -band magnitude directly reflects the bolometric magnitude (e.g. Wood et al. 1992). But many IRAS detected stars are optically thick in the K -band, and can become as faint as $K > 15$ mag for $M_{\text{bol}} \sim -5$ mag. Even RSGs are found at $K > 10$ mag.

Frogel & Richer (1983) searched for obscured stars down to a completeness limit of $K = 11$ mag, and according to Fig. 6 they would have missed a significant fraction of the obscured AGB stars. Frogel et al. (1990) searched for AGB stars in MC clusters down to a limiting magnitude varying between $K = 12$ and 13. Wood et al. (1992) searched for IRAS counterparts down to a lim-

iting magnitude of $K = 12.5$. Neither of them are complete for obscured AGB stars. Most of the newly found obscured AGB stars in paper III have $K > 12.5$ mag, and we cannot exclude the possible existence of IRAS detected AGB stars in the LMC at $K > 17$ mag. It is unlikely that these stars have $M_{\text{bol}} < -6$ mag. There are still some 200 IRAS point sources, however, which are candidate mass-losing AGB stars in the LMC (paper I), but which have not been adequately imaged at NIR wavelengths. These may include stars with $M_{\text{bol}} < -6$ mag. Hence the apparent lack of luminous mass-losing AGB stars in the LMC may well be a result of incompleteness.

Selection effects could have been introduced by the detection limits in the IRAS 12 and 25 μm bands, and by the detection limits of the ground-based instruments that were used to search for counterparts — mainly at NIR wavelengths. These effects are difficult to quantify, since the IR properties of obscured carbon and oxygen stars are not yet known as a function of their bolometric luminosities. The completeness of our sample of obscured AGB stars is essentially limited by the IRAS sensitivity at 25 μm (paper II), i.e. it is probably not affected much by the contribution of the 10 μm SiO feature in oxygen-rich CSEs to the IRAS 12 μm flux-density. The emissivities of carbon- and oxygen-rich dust differ in such a way that a carbon star, with the same luminosity and mass-loss rate as an oxygen-rich star, will be brighter at 25 μm and fainter in the NIR than its oxygen-rich counterpart. Thus IRAS may have detected carbon-rich stars to slightly lower luminosities than oxygen-rich ones, at 25 μm . However, the same effect will render our NIR searches slightly less sensitive to carbon stars than to oxygen stars. At present it is not clear what the resulting selection effect is. We feel that selection effects may become important at $M_{\text{bol}} > -5$ mag.

8.2. Mid-IR variability

The amplitude of the N -band variations is surprisingly large: 1.4 mag (peak-to-peak). Harvey et al. (1974) found a mean 10 μm amplitude of 0.88 ± 0.13 mag for a sample of galactic OH/IR stars and Le Bertre (1993) found a mean N -band amplitude of 1.01 ± 0.13 mag for a sample of galactic mass-losing oxygen-stars. Le Bertre (1992) found a smaller mean N -band amplitude of 0.61 ± 0.10 mag for a similar sample of carbon stars.

Harvey et al. (1974) found a mean K -band amplitude of 1.13 ± 0.16 mag for the galactic OH/IR stars that they monitored at 10 μm . Le Bertre (1992, 1993) found a mean K -band amplitude of 1.08 ± 0.14 mag for the galactic mass-losing oxygen stars and a similar mean K -band amplitude of 1.13 ± 0.16 mag for galactic mass-losing carbon-stars, that he monitored in the N -band. This is comparable to the stars for which we had two N -band measurements and that have a K -band amplitude of 1.1 mag.

Le Bertre (1988, 1992, 1993) concludes that the mid-IR variability is due to changes of the bolometric luminosity. The $10\ \mu\text{m}$ amplitude of oxygen stars has an additional component due to variations of the SiO dust feature. The LMC stars with two N -band measurements have the $10\ \mu\text{m}$ SiO feature in emission, whereas galactic OH/IR stars show it in (self-)absorption. As an emission feature is more sensitive to changes in optical depth and luminosity than a (self-)absorbed feature, this may explain the large N -band amplitude of the oxygen-rich mass-losing LMC stars compared to their galactic counterparts — especially the galactic OH/IR stars.

Our data suggests a phase lag of ~ 0.13 pulsation period between the K - and N -band light-curves. This seems to be at odds with the findings for the galactic obscured LPVs that the IR light-curves between ~ 1 and $12\ \mu\text{m}$ are all in phase with each other (e.g. Nyman & Olofsson 1986; Jewell et al. 1991), lagging the optical light-curve by between ~ 0.1 and 0.2 times the period. The discrepancy may be explained by the fact that the stars we investigated do not have extremely optically-thick CSEs. The observed phase-lag between the K - and N -band light curves may reflect a correlation between the emission strength of the $10\ \mu\text{m}$ SiO feature, and the optical radiation field. We find a clear indication that the variability of $(K - [12])$ decreases with increasing $(K - [12])$ colour, i.e. with increasing optical depth of the CSE. Hence the phase lag between the K - and N -band light-curves may disappear in the most extremely obscured sources, where the $10\ \mu\text{m}$ feature turns into (self-)absorption.

8.3. Frequency of carbon stars

For the sample of IRAS detected AGB stars in the LMC the ratio of the number of carbon stars to oxygen stars is in the range 0.21 to 0.83 depending on the number of carbon stars among the OC stars. If the lower value is correct, the ratio depends only weakly on luminosity, whereas the higher value would imply a ratio that steeply decreases with increasing luminosity. The probability that an obscured AGB star is a carbon star most likely decreases from $\sim 40\%$ at $M_{\text{bol}} = -5$ mag ($\log(L/L_{\odot}) = 3.9$), to $\sim 20\%$ at $M_{\text{bol}} = -7$ mag ($\log(L/L_{\odot}) = 4.7$). At the lower luminosity end ($\log(L/L_{\odot}) = 3.9$) the fraction of carbon stars is constrained to be between ~ 22 and 57% . At the other extreme, carbon stars are not completely absent amongst the most luminous AGB stars.

How does this result compare with the luminosity distributions of optically visible AGB stars in the LMC? Groenewegen & de Jong (1993) used a synthetic evolution model to reproduce the observed optically visible carbon star luminosity function (Cohen et al. 1981; Richer et al. 1979; see also Costa & Frogel 1996) as well as the number ratio between carbon and oxygen stars (Blanco & McCarthy 1983). They find a mean ratio of the number of carbon stars to the number of oxygen stars of 0.85, in good

agreement with the observed range of 0.6 to 2.2 for the optically visible AGB stars. Amongst the sample of obscured AGB stars in the LMC carbon stars are less common than they are amongst optically visible AGB stars. The number of optically visible AGB stars steeply declines between $M_{\text{bol}} = -5$ and -6 mag. The obscured AGB star distribution peaks near $M_{\text{bol}} = -5.8$ mag, and has a gradual high-luminosity drop-off. Thus the fraction of obscured stars amongst the AGB stars increases with bolometric luminosity. This is to be expected when optically visible AGB stars still evolve along the AGB, thereby significantly increasing in luminosity before becoming dust-enshrouded.

8.4. The most luminous AGB stars

The Chandrasekhar limit to the stellar core mass of $1.4M_{\odot}$ corresponds, via the core mass-luminosity relation, to an AGB luminosity limit of $M_{\text{bol}} \sim -7$ mag (Paczynski 1971). However, in recent years it has been suggested that for some intermediate-mass stars the core mass-luminosity relation may not be valid near the tip of the AGB, if AGB stars become more luminous as a result of HBB (e.g. Blöcker & Schönberner 1991; Blöcker 1995; Marigo et al. 1996). On the other hand, Reid et al. (1990) argue that, as a result of intense mass loss on the upper AGB, stars may not actually become much more luminous than $M_{\text{bol}} \sim -6$ mag.

We discovered that with $M_{\text{bol}} \sim -6.8$ mag, the LMC star IRAS04496–6958 is the most luminous carbon star known in the MCs. Other luminous mass-losing carbon stars in the MCs are IRAS06028–6722 (LI-LMC1817) with $M_{\text{bol}} \sim -6.1$ mag in the LMC (paper III), and IRAS00554–7351 with $M_{\text{bol}} \sim -6.0$ mag in the SMC (Whitelock et al. 1989; Wood et al. 1992). IRAS00350–7436 in the SMC may also be a carbon star: Whitelock et al. (1989) found that it has a K-type spectrum with weak C_2 absorption bands, and they explain this object as being either a carbon-rich post-AGB object in the transition to the planetary nebula phase, or an interacting binary. We estimate $M_{\text{bol}} \sim -6.8$ mag, i.e. equally luminous as IRAS04496–6958. Confirmation that IRAS00350–7436 has become carbon enriched due to dredge-up is crucial.

The two brightest LMC stars in our TIMMI sample are IRAS04498–6842 and IRAS05329–6709, both probable oxygen stars. In 1994 November they were very luminous: $M_{\text{bol}} \sim -8.2$ and -7.6 mag respectively. For IRAS05329–6709 this may be due to variability: compare the NIR brightness in 1994 November to its light curve (Wood et al. 1992). The NIR variability of IRAS04498–6842 suggests it is a Mira variable, while its rather blue ($H - K$) colour is more characteristic of a RSG. With $M_{\text{bol}} \sim -7.2$ and -6.7 mag, IRAS04509–6922 and IRAS04516–6902 are amongst the most luminous AGB stars, and our optical/NIR spectra have shown them to be oxygen rich. IRAS05316–6604 (WOH SG374) was listed in paper II as an AGB star can-

didate with $M_{\text{bol}} \sim -7.2$ mag, but its near/mid-IR colours suggest it may be a RSG.

IRAS00165–7418 (VV Tuc) is probably a RSG, judging from its high bolometric luminosity ($M_{\text{bol}} \sim -9.1$ mag) and its location in the $(K - [12])$ versus $(H - K)$ diagram. The oxygen-rich nature of IRAS01074–7140 ($M_{\text{bol}} \sim -7.0$ mag) is in agreement with its spectral type of M5e (White-lock et al. 1989).

8.5. Hot Bottom Burning

It has been proposed that in AGB stars with massive mantles, the convective layer may reach the nuclear burning shells. This so-called Hot Bottom Burning (HBB; e.g. Boothroyd et al. 1995, and references therein) could prevent stars with progenitor masses ~ 6 to $7M_{\odot}$ and solar metallicity from becoming carbon stars, and may increase their bolometric luminosities by an unknown factor. For half solar metallicity — which is typical for the LMC (Russell & Bessell 1989; Russell & Dopita 1990) — this may occur in AGB stars with a progenitor mass as low as $\sim 5M_{\odot}$.

Reid et al. (1988, 1995) did not find any carbon star brighter than $M_{\text{bol}} = -6$ mag amongst their LMC LPVs. However, we find IRAS04496–6958 to be a very luminous, $M_{\text{bol}} = -6.8$ mag, carbon star. At this luminosity AGB stars are expected to be oxygen rich due to the effects of HBB. On the other hand, we also find oxygen-rich AGB stars with luminosities as faint as $M_{\text{bol}} \sim -5$ mag, where mass-losing AGB stars are expected to be carbon rich.

Intense mass loss decreases the mass contained in the stellar mantle, and HBB may switch off. Hence very luminous AGB stars may become carbon-rich again, just before they leave the AGB. The possibly very luminous carbon-rich post-AGB object IRAS00350–7436 (see above) may be an example of this scenario.

9. Conclusions

We have studied the chemical composition of the photospheres and circumstellar envelopes of the presently known sample of obscured (i.e. IRAS detected) AGB stars in the LMC. Because of their high mass-loss rates these stars are expected to be representative of AGB stars upon termination of their evolution along the AGB. Thus they are different from optically visible AGB stars, which may still evolve in luminosity and photospheric chemical composition before leaving the AGB. The bolometric luminosity should therefore be a much better measure of the main-sequence mass for an obscured AGB star, than it is for an optically visible AGB star.

Our search for new OH maser emitters in the LMC resulted in one new detection, from IRAS04407–7000. For two stars with moderately thick CSEs spectra around 800 nm were obtained. For the remainder of the sample, we used the $(K - [12])$ versus $(H - K)$ diagram to establish

the probable chemical composition of their CSEs. The diagram may also distinguish between RSGs and AGB stars: RSGs have optically thinner CSEs (bluer $(H - K)$ colours) than do AGB stars, at the same $12 \mu\text{m}$ excess with respect to the K -band magnitude. This is because RSGs are bigger than AGB stars, and so are the inner radii of their respective CSEs.

The ratio of the number of carbon stars to the number of oxygen stars is found to decrease with increasing luminosity. Carbon stars are very rare at luminosities exceeding $M_{\text{bol}} \sim -6$ mag, but not absent. The most luminous carbon star in the MCs is found to be IRAS04496–6958, with $M_{\text{bol}} = -6.8$ mag. Yet there are still many mass-losing stars at luminosities about $M_{\text{bol}} \sim -5$ mag that are oxygen rich. It is puzzling to find carbon stars and oxygen stars at the same luminosity at the tip of the thermally pulsing AGB. Possibly the sample of mass-losing AGB stars represents a range of metallicities (cf. Olszewski et al. 1996), in which case the luminous carbon stars would be metal rich and therefore not experience HBB, whereas the less luminous oxygen stars would be metal poor and therefore already experience HBB at low luminosities.

Acknowledgements. We would like to thank Peter Wood for providing us with data on his OH/IR and SHV stars, Hans-Ulrich Käuffel for helping with the observations of the TIMMI standard stars, Jay Frogel for critically reading the manuscript, and the referee Prof. Harm Habing for his comments which helped improve the paper. We acknowledge the granting of Director’s Discretionary Time for obtaining the NTT spectra. Jacco lamenta de estar deprivado de la mejor manera para agradecer a Montse como ella lo merecio mas que nadie.

A. TIMMI standard stars

On 1995 December 4 and 5 we measured several standard stars, in order to examine the quality of the currently available standard-star magnitudes. The results are presented in Table 7 for the broad- ($N = N_0$) and narrow-band ($N_{1,2,3}$) magnitudes. The N_1 , N_2 , and N_3 filters are centred at 8.4, 9.8, and $12.6 \mu\text{m}$, respectively (<http://www.eso.org/proposals/timmi.html>). We quote the magnitudes that have been in use at ESO from a compilation by Koornneef & Yagnam (ESO, 1985, unpublished) as well as more recent measurements, obtained with the ESO InSb bolometer by van der Blik et al. (1996). The bright stars α CMa (Sirius) and α Car (Canopus) were adopted as standards for the broad- and narrow-band magnitudes respectively; using the magnitudes given by van der Blik et al. (1996). The stars γ Ret and λ Vel are suspected by Koornneef & Yagnam to be variable. This would not be surprising for a giant of a spectral type as late as M4 (γ Ret) or a late-type supergiant (λ Vel).

By studying the airmass dependence of the differences between our photometry and that by van der Blik et al. (1996) we estimated the atmospheric extinction coefficients. For the N_0 -band these coefficients were 0.50 and 0.46 mag/airmass for the first and second night respectively. For the N_1 , N_2 , and N_3 -bands on the second night the coefficients were 0.36, 0.38, and 0.40 mag/airmass respectively.

Table 7. Magnitudes of TIMMI standard stars: Bright Star Catalogue entries, names, spectral types, magnitude band (N_0 , N_1 , N_2 , or N_3), and magnitudes: Koornneef & Yagnam (ESO, 1985, unpublished), van der Blik et al. (1996), and our observations, with their 1- σ error estimates (where known). We adopted the magnitudes from van der Blik et al. for α CMa (N_0) and α Car ($N_{1,2,3}$).

BSC entry	Name	Spectral type	magnitude band	Koornneef & Yagnam	van der Blik et al.	this paper
HR 1264	γ Ret	M4 III	N_0	-0.71	-0.73 ± 0.03	-0.87 ± 0.03
			N_1	-0.65	-0.64 ± 0.02	-0.75 ± 0.04
			N_2	-0.73	-0.74 ± 0.01	-0.85 ± 0.04
			N_3	-0.80	-0.82 ± 0.02	-0.93 ± 0.04
HR 2326	α Car	F0 II	N_0	-1.52	-1.46 ± 0.02	-1.44 ± 0.02
			N_1	-1.51	-1.45 ± 0.02	adopted
			N_2	-1.52	-1.47 ± 0.02	adopted
			N_3	-1.45	-1.44 ± 0.02	adopted
HR 2491	α CMa	A1 v	N_0	-1.41	-1.40 ± 0.02	adopted
HR 3634	λ Vel	K4 Ib-II	N_0	-1.78	-1.77 ± 0.02	-1.76 ± 0.02
HR 3748	α Hya	K3 II-III	N_0	-1.30	-1.30 ± 0.01	-1.39 ± 0.02
HR 3903	ν Hya	G7 III(b)	N_0			1.74 ± 0.02
HR 4174	γ Cha	M0 III	N_0			-0.14 ± 0.04

Our observed magnitude for λ Vel is in excellent agreement with those found by the above mentioned authors, although it is a suspected variable. Late-type supergiants are generally less variable than are AGB stars. There is less agreement about the magnitudes of α Car, α Hya (Alphard) and especially γ Ret. It is not likely that the discrepancy for γ Ret has to do with the differences in the spectral response functions of the bolometer and the camera: λ Vel and γ Ret have similar spectral slopes within the N -band, as seen from their N_1 -, N_2 -, and N_3 -band magnitudes (Table 7). It is more likely that γ Ret is indeed variable. Our N_0 -band magnitude of α Car confirms the result by van der Blik et al. (1996). Either this star is variable, or the magnitude listed by Koornneef & Yagnam is incorrect. Van der Blik et al. (1996) do agree with Koornneef & Yagnam on the N_0 -band magnitude of α Hya, whereas we measure it to be brighter by 0.09 mag. The SAAO NIR standard stars ν Hya and γ Cha (Carter & Meadows 1995) have been observed for the first time in the N -band, and they may be suitable for use as standard stars if they are confirmed to be non-variable. Both are fainter than the standards currently in use.

We conclude that it is difficult to obtain photometric accuracies better than ~ 5 or 10% in the N -band with TIMMI, as the accuracy is limited by the reliability of the available standard star values. The error in an individual measurement for a star with N between ~ 3 and ~ 4 mag is dominated by the uncertainty in the adopted magnitude of the standard star used. Measurements of stars fainter than $N \sim 6$ mag are dominated by the intrinsic noise in the measurement. Together with uncertainties involved in the extinction correction, this combines with the internal noise on an individual measurement into the 1- σ error estimates given in Table 1.

B. IR colour relations

We have investigated the IR colour relations for the J , H , K , and L -bands in the SAAO photometric system, and the IRAS 12 and 25 μm bands. We define $[12] = -2.5 \log(S_{12}/28.3)$ and $[25] = -2.5 \log(S_{25}/6.73)$, where S_{12} and S_{25} are the flux densities in Jy at 12 and 25 μm , respectively (IRAS Explanatory

Supplement 1988). The SAAO L -band has an effective wavelength of 3.45 μm .

We plot the $(J - H)$, $(K - L)$, and $([12] - [25])$ colours versus the $(H - K)$ colour (Fig. 7). The dotted lines are linear fits to the data points:

$$\begin{pmatrix} (J - H) \\ (K - L) \\ ([12] - [25]) \end{pmatrix} = \begin{pmatrix} 0.51 \pm 0.43 \\ 0.12 \pm 0.30 \\ 1.57 \pm 0.49 \end{pmatrix} + \begin{pmatrix} 1.08 \pm 0.17 \\ 1.15 \pm 0.09 \\ 0 \end{pmatrix} \times (H - K) \quad (\text{B1})$$

Cohen et al. (1981) showed that the $(H - K)$ and $(J - H)$ colours of optically visible carbon stars in the Milky Way are correlated, from which we derive on the SAAO system (Carter 1990):

$$(J - K) = 0.76 + 1.95 \times (H - K) \quad (\text{B2})$$

They explained the correlation as a result of line blanketing by molecular absorption bands. From Costa & Frogel (1996) we derive a correlation between their $(J - K)$ and $(H - K)$ colours, transformed to the SAAO system (Carter 1990), for optically visible carbon stars in the LMC:

$$(J - K) = 0.77 + 1.83 \times (H - K) \quad (\text{B3})$$

The selected sample of Milky Way stars from Guglielmo et al. (1993) yield, after transformation to the SAAO system (Carter 1990), for the obscured carbon stars:

$$(J - K) = (0.81 \pm 0.29) + (2.29 \pm 0.03) \times (H - K) \quad (\text{B4})$$

and for the obscured oxygen stars:

$$(J - K) = (0.70 \pm 0.26) + (2.43 \pm 0.03) \times (H - K) \quad (\text{B5})$$

For the obscured AGB stars in the LMC we derive:

$$(J - K) = (0.51 \pm 0.43) + (2.08 \pm 0.17) \times (H - K) \quad (\text{B6})$$

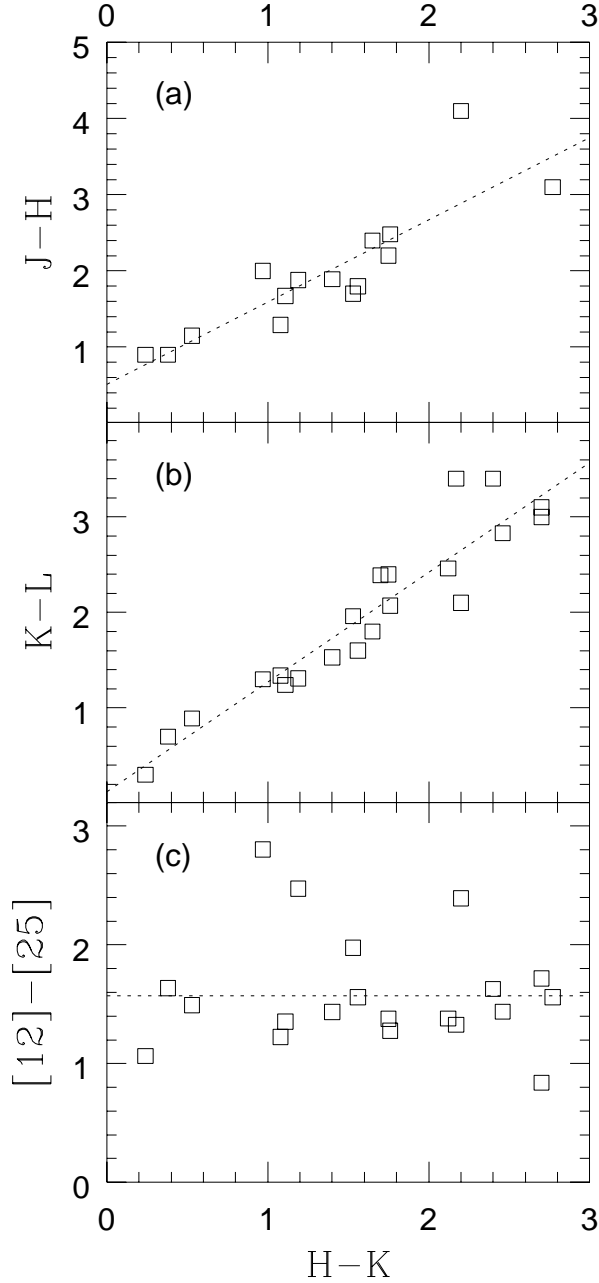


Fig. 7. ($J - H$) (a), ($K - L$) (b), and ($[12] - [25]$) (c) colours versus ($H - K$) colour for the stars of our sample. The dotted lines are linear fits to the data

We plot K and N -band magnitudes and ($H - K$) and ($K - [12]$) colours versus the bolometric luminosity (Fig. 8). The dotted lines are linear fits to the LMC data points (we also include the stars with N -band lower limits, to diminish bias):

$$\begin{pmatrix} K \\ (H - K) \\ N \\ (K - N) \end{pmatrix} = \begin{pmatrix} 18.9 \pm 1.0 \\ 3.6 \pm 0.6 \\ 10.6 \pm 0.4 \\ 8.4 \pm 1.1 \end{pmatrix} + \begin{pmatrix} 1.35 \pm 0.26 \\ 0.29 \pm 0.16 \\ 0.87 \pm 0.10 \\ 0.47 \pm 0.28 \end{pmatrix} \times M_{\text{bol}}(\text{B7})$$

Bolometrically fainter stars are relatively fainter in the K -band, and relatively brighter in the N -band, yielding larger

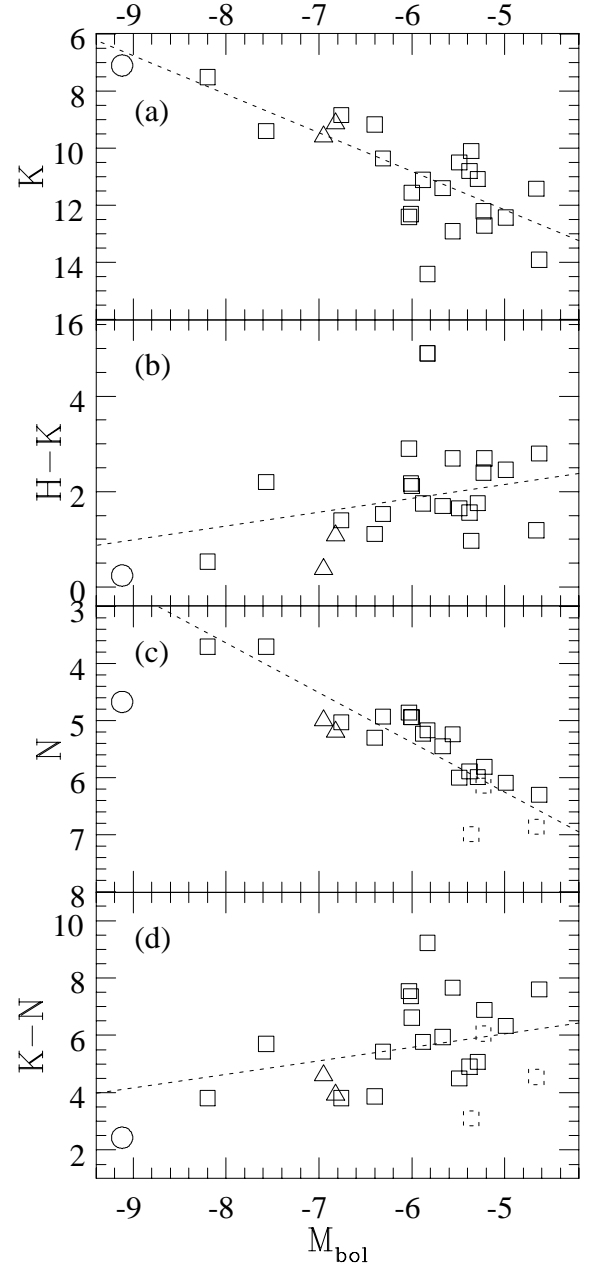


Fig. 8. K (a), ($H - K$) (b), N (c), and ($K - [12]$) (d) as a function of absolute bolometric magnitude for the LMC stars (squares, dotted in the case of lower limits to the N -band magnitudes and upper limits to the ($K - N$) colours, respectively), SMC stars (triangles), and VV Tuc (circle). The dotted lines are linear fits to the LMC data (see text)

($K - [12]$) colours. Their ($H - K$) colours are also larger, indicating that fainter stars are optically thicker: at equal mass-loss rates, they have smaller inner radii of the CSEs, and consequently larger dust column densities than the more luminous stars. Thus fainter stars have fainter K -band magnitudes due to increased circumstellar opacity, and brighter N -band magnitudes due to increased circumstellar dust emission.

References

- Allain D., Bica E., 1989, *A&A* 217, 57
- Barnbaum C., Stone R.P.S., Keenan P.C., 1996, *ApJS* 105, 419
- Blanco V.M., McCarthy M.F., Blanco B.M., 1980, *ApJ* 242, 938
- Blanco V.M., McCarthy M.F., 1983, *AJ* 88, 1442
- Blöcker T., 1995, *A&A* 297, 727
- Blöcker T., Schönberner D., 1991, *A&A* 244, L43
- Boothroyd A.I., Sackmann I.-J., Wasserburg G.J., 1995, *ApJ* 442, L21
- Caputo F., 1997, *MNRAS* 284, 994
- Carter B.S., 1990, *MNRAS* 242, 1
- Carter B.S., Meadows V.S., 1995, *MNRAS* 276, 734
- Cohen J.G., Frogel J.A., Persson S.E., Elias J.H., 1981, *ApJ* 249, 481
- Costa E., Frogel J.A., 1996, *AJ* 112, 2607
- Couture J., Hardy E., 1993, *ApJ* 406, 142
- Crotts A.P.S., Kunkel W.E., Heathcote S.R., 1995, *ApJ* 438, 724
- Danks A.C., Dennefeld M., 1994, *PASP* 106, 382
- Elias J.H., Frogel J.A., Humphreys R.M., 1985, *ApJS* 57, 91
- Elias J.H., Frogel J.A., Schwing P.B.W., 1986, *ApJ* 302, 675
- Feast M.W., 1996, *MNRAS* 278, 11
- Feast M.W., 1997, *MNRAS* 284, 761
- Feast M.W., Robertson B.S.C., Catchpole R.M., Lloyd Evans T., Glass I.S., Carter B.S., 1982, *MNRAS* 201, 439
- Feast M.W., Walker A.R., 1987, *ARA&A* 25, 345
- Feast M.W., Catchpole R.M., 1997, *MNRAS* (in press)
- Fluks M.A., Plez B., Thé P.S., de Winter D., Westerlund B.E., Steenman H.C., 1994, *A&AS* 105, 311
- Fluks M.A., Thé P.S., Westerlund B.E., 1997, *A&A* (submitted)
- Frogel J.A., Richer H.B., 1983, *ApJ* 275, 84
- Frogel J.A., Mould J., Blanco V.M., 1990, *ApJ* 352, 96
- Gallagher J.S., Mould J.R., De Feijter E., Holtzman J., Stappers B., Watson A., Trauger J., Ballester G.E., Burrows C.J., Casertano S., Clarke J.T., Crisp D., Griffiths R.E., Hester J.J., Hoessel J., Krist J., Matthews L.D., Scowen P.A., Stapelfeld K.R., Westphal J.A., 1996, *ApJ* 466, 732
- Glass I.S., Feast M.W., 1973, *MNRAS* 163, 245
- Green P., 1997. In: Wing R.F. (ed.) *The Carbon Star Phenomenon*. Kluwer, Dordrecht
- Groenewegen M.A.T., de Jong T., 1993, *A&A* 267, 410
- Groenewegen M.A.T., Smith C.H., Wood P.R., Omont A., Fujiyoshi T., 1995, *ApJ* 449, L119
- Guglielmo F., Epchtein N., Le Bertre T., Fouqué P., Hron J., Kerschbaum F., Lépine J.R.D., 1993, *A&AS* 99, 31
- Habing H.J., 1996, *A&AR* 7, 97
- Harvey P.M., Bechis K.P., Wilson W.J., Ball J.S., 1974, *ApJS* 27, 331
- Hodge P.W., Sexton J.A., 1966, *AJ* 71, 363
- Hughes S.M.G., Wood P.R., 1990, *AJ* 99, 784
- Iben I., 1981, *ApJ* 246, 278
- Iben I., Renzini A., 1983, *ARA&A* 21,271
- Jaschek C., Jaschek M., 1987, *The classification of stars*. Cambridge University Press, Cambridge
- Jewell P.R., Snyder L.E., Walmsley C.M., Wilson T.L., Gensheimer P.D., 1991, *A&A* 242, 211
- Joint IRAS Science Working Group, 1988. Beichman C.A., Neugebauer G., Habing H.J., Clegg P.E., Chester T.J. (eds.) *Infrared Astronomical Satellite, Catalogs and Atlases, Explanatory Supplement*.
- Käufel U., Jouan R., Lagage P.O., Masse P., Mestreau P. Tarrus A., 1992, *The Messenger*, 70, 67
- Keenan P.C., 1993, *PASP* 105, 905
- Le Bertre T., 1988, *A&A* 190, 79
- Le Bertre T., 1992, *A&AS* 94, 377
- Le Bertre T., 1993, *A&AS* 97, 729
- Lidman C., 1995, *IRAC-2b Report on Test Observations III. ESO*
- Loup C., Zijlstra A.A., Waters L.B.F.M., Groenewegen M.A.T., 1997, *A&AS* (paper I, in press)
- Marigo P., Girardi L., Chiosi C., 1996, *A&A* 316, L1
- McGregor P.J., 1994, *PASP* 106, 508
- Nyman L.-Å., Olofsson H., 1986, *A&A* 158, 67
- Olszewski E.W., Suntzeff N.B., Mateo M., 1996, *ARA&A* 34, 511
- Paczyński B., 1971, *Acta Astron.* 21, 417
- Reid I.N., 1991, *ApJ* 382, 143
- Reid I.N., Glass I.S., Catchpole R.M., 1988, *MNRAS* 232, 53
- Reid I.N., Tinney C.G., Mould J.R., 1990, *ApJ* 348, 98
- Reid I.N., Hughes S.M.G., Glass I.S., 1995, *MNRAS* 275, 331
- Richer H.B., Olander N., Westerlund B.E., 1979, *ApJ* 230, 724
- Russell S.C., Bessell M.S., 1989, *ApJS* 70, 865
- Russell S.C., Dopita M.A., 1990, *ApJS* 74, 93
- Sonneborn G., Fransson C., Lundqvist P., Cassatella A., Gilmozzi R., Kirshner R.P., Panagia N., Wamsteker W., 1997, *ApJ* 477, 848
- Sterken C., Manfroid J., 1992, *Astronomical photometry, a guide*. Kluwer, Dordrecht, p. 262
- Turnshek D.E., Turnshek D.A., Craine E.R., Boeshaar P.C., 1985, *An atlas of digital spectra of cool stars*. Western Research Company, Tucson
- Van der Blik N.S., Manfroid J., Bouchet P., 1996, *A&AS* 119, 547
- Van der Veen W.E.C.J., 1989, *A&A* 210, 127
- Van Leeuwen F., Feast M.W., Whitelock P.A., Yudin B., 1997, *MNRAS* 287, 955
- Van Loon J.Th., Zijlstra A.A., Bujarrabal V., Nyman L.-Å., 1996, *A&A* 306, L29
- Van Loon J.Th., Zijlstra A.A., Whitelock P.A., Waters L.B.F.M., Loup C., Trams N., 1997, *A&A* (paper III, in press)
- Westerlund B.E., Olander N., Hedin B., 1981, *A&AS* 43, 267
- Whitelock P.A., Feast M.W., Menzies J.W., Catchpole R.M., 1989, *MNRAS* 238, 769
- Whitelock P.A., Menzies J.W., Feast M.W., Catchpole R.M., Marang F., Carter B.S., 1995, *MNRAS* 276, 219
- Wood P.R., Whiteoak J.B., Hughes S.M.G., Bessell M.S., Gardner F.F., Hyland A.R., 1992, *ApJ* 397, 552
- Zijlstra A.A., Loup C., Waters L.B.F.M., Whitelock P.A., van Loon J.Th., Guglielmo F., 1996, *MNRAS* 279, 32 (paper II)